Hypomorphic Mutations in *TONSL* Cause SPONASTRIME Dysplasia

Hae Ryung Chang,[1,19] Sung Yoon Cho,[2,19] Jae Hoon Lee,[3,19] Eunkyung Lee,[1,19] Jieun Seo,[4] Hye Ran Lee,[5] Denise P. Cavalcanti,[6] Outi Mäkitie,[7] Helena Valta,[7] Katta M. Girisha,[8] Chung Lee,[9] Kausthubham Neethukrishna,[8] Gandham S. Bhavani,[8] Anju Shukla,[8] Sheela Nampoothiri,[10] Shubha R. Phadke,[11] Mi Jung Park,[12] Shiro Ikegawa,[13] Zheng Wang,[13,14] Martin R. Higgs,[15] Grant S. Stewart,[15] Eunyoung Jung,[1] Myeong-Sok Lee,[1] Jong Hoon Park,[1] Eun A. Lee,[16] Hongtae Kim,[16] Kyungjae Myung,[16] Woosung Jeon,[17] Kyoungyeul Lee,[17] Dongsup Kim,[17] Ok-Hwa Kim,[18] Murim Choi,[4] Han-Woong Lee,[3,20] Yonghwan Kim,[1,20,*] and Tae-Joon Cho[5,20,*]

SPONASTRIME dysplasia is a rare, recessive skeletal dysplasia characterized by short stature, facial dysmorphism, and aberrant radiographic findings of the spine and long bone metaphysis. No causative genetic alterations for SPONASTRIME dysplasia have yet been determined. Using whole-exome sequencing (WES), we identified bi-allelic *TONSL* mutations in 10 of 13 individuals with SPONASTRIME dysplasia. TONSL is a multi-domain scaffold protein that interacts with DNA replication and repair factors and which plays critical roles in resistance to replication stress and the maintenance of genome integrity. We show here that cellular defects in dermal fibroblasts from affected individuals are complemented by the expression of wild-type *TONSL*. In addition, *in vitro* cell-based assays and *in silico* analyses of TONSL structure support the pathogenicity of those *TONSL* variants. Intriguingly, a knock-in (KI) *Tonsl* mouse model leads to embryonic lethality, implying the physiological importance of TONSL. Overall, these findings indicate that genetic variants resulting in reduced function of TONSL cause SPONASTRIME dysplasia and highlight the importance of TONSL in embryonic development and postnatal growth.

Introduction

SPONASTRIME dysplasia (MIM: 271510), the denotation of which originates from "spondylar and nasal alterations with striated mataphyses,"[1] is a very rare but distinct entity that can be categorized as a spondyloepimetaphyseal dysplasia that is transmitted as an autosomal-recessive trait. To date, only 15 individuals with this disorder have been reported[1–10] on the basis of the diagnostic criteria, suggested by Langer et al.,[5] that consist of a unique combination of clinical and radiological findings. The major clinical features are mild to moderate short-limb type dwarfism and a relatively large head with a prominent forehead, as well as epicanthic folds observed in infancy or early childhood. However, the clinical criteria are nonspecific and radiological features must be present for a diagnosis. Diagnostic criteria based on the radiological features focus on the changes in the lumbar vertebrae and metaphyseal changes in the long bones. Metaphyseal irregularities and striations, as proposed by the disease's name, are also important diagnostic criteria, but they are not seen as consistently as the lumbar vertebral changes.[5] To date, causative genetic mutations for SPONASTRIME dysplasia have not been determined, and thus a genetic test for this disease is not yet clinically available.

Tonsoku-like DNA repair protein (TONSL) is a multi-domain scaffold protein that interacts with DNA replication and repair factors, including anti-silencing function 1 (ASF1), minichromosome maintenance complex component helicases (MCM helicases), H3 histone, H4 histone, and MMS22-like protein (MMS22L).[11–15] TONSL consists of 1,378 amino acids, such as eight tetratricopeptide repeats (TPR), three Ankyrin (ANK) repeats, an ubiquitin-like domain (UBL), and seven leucine-rich repeats (LRR),

[1]Department of Biological Sciences, Sookmyung Women's University, Seoul 04310, Republic of Korea; [2]Department of Pediatrics, Samsung Medical Center, Sungkyunkwan University School of Medicine, Seoul 06351, Republic of Korea; [3]Department of Biochemistry, Yonsei University, Seoul 03722, Republic of Korea; [4]Department of Biomedical Sciences, Seoul National University College of Medicine, Seoul 03080, Republic of Korea; [5]Department of Orthopaedic Surgery, Seoul National University College of Medicine, Seoul 03080, Republic of Korea; [6]Department of Medical Genetics, Faculty of Medical Sciences, University of Campinas, Campinas, São Paulo 13083-887, Brazil; [7]Children's Hospital, University of Helsinki and Helsinki University Hospital, Helsinki 00290, Finland; [8]Department of Medical Genetics, Kasturba Medical College, Manipal Academy of Higher Education, Manipal, Karnataka 576104, India; [9]Samsung Genome Institute, Samsung Medical Center, Seoul 06351, Republic of Korea; [10]Department of Pediatric Genetics, Amrita Institute of Medical Sciences and Research Centre, Cochin, Kerala 682041, India; [11]Department of Medical Genetics, Sanjay Gandhi Postgraduate Institute of Medical Sciences, Lucknow, Uttar Pradesh 226014, India; [12]Department of Pediatrics, Inje University Sanggye Paik Hospital, Seoul 01757, Republic of Korea; [13]Laboratory for Bone and Joint Diseases, RIKEN Center for Integrative Medical Sciences, Tokyo 108-8639, Japan; [14]McKusick-Zhang Center for Genetic Medicine and State Key Laboratory of Medical Molecular Biology, Institute of Basic Medical Sciences, Chinese Academy of Medical Sciences and Peking Union Medical College, Beijing 100005, People's Republic of China; [15]Institute of Cancer and Genomics Sciences, University of Birmingham, Birmingham, West Midlands B15 2TT, UK; [16]Center for Genomic Integrity, Institute for Basic Science, Ulsan National Institute of Science and Technology, Ulsan 44919, Republic of Korea; [17]Department of Bio and Brain Engineering, Korean Advanced Institute of Science and Technology, Daejeon 34141, Republic of Korea; [18]Department of Radiology, Woorisoa Children's Hospital, Seoul 08291, Republic of Korea
[19]These authors contributed equally to this work
[20]These authors contributed equally to this work
*Correspondence: tjcho@snu.ac.kr (T.-J.C.), yhkim@sookmyung.ac.kr (Y.K.)
https://doi.org/10.1016/j.ajhg.2019.01.009.

with annotated domains.[13] It was reported that the TONSL-MMS22L heterodimer plays a key role in the homologous recombination required for repairing spontaneous replication-associated DNA lesions. At the cellular level, depleting TONSL causes pronounced defects in the rate of cell proliferation and enhances sensitivity to camptothecin (CPT), a topoisomerase 1 inhibitor that induces DNA breakage at replication forks.[12,13] Specifically, TONSL-MMS22L is recruited to the sites of stalled replication forks during normal S phase by replication protein A (RPA1, RPA2, and RPA3) bound to single-strand DNA (ssDNA), and it promotes RAD51 loading for strand invasion.[16] Therefore, it was demonstrated that small interfering RNA (siRNA)-mediated TONSL knockdown leads to the loss of damage-induced RAD51-foci formation in cells treated with genotoxic agents.[11,12,16]

In this study, in order to identify the causative genetic alteration for SPONASTRIME dysplasia, we recruited 13 individuals, including one whose case had been previously reported,[10] from four different ethnicities; all of these individuals satisfied the diagnostic criteria of the disease. By performing whole-exome sequencing (WES) and Sanger sequencing, we identified autosomal-recessive hypomorphic and loss-of-function (LoF) mutations in the *TONSL* (MIM: 604546) gene of individuals with SPONASTRIME dysplasia. In further studies, using dermal fibroblasts from affected individuals, *in vitro* cell-based assays, *in silico* structure simulation, and an *in vivo* knock-in (KI) mouse model, we demonstrated the pathogenicity of *TONSL* variants, suggesting that defects in replication-associated DNA-damage repair and the resultant inefficient cell proliferation due to *TONSL* mutations might be the underlying pathogenic mechanism for SPONASTRIME dysplasia.

Material and Methods

Subjects

Written informed consent was obtained from the affected individuals or their parents. The institutional review boards of the Seoul National University Hospital, Seoul, Republic of Korea and Samsung Medical Center, Seoul, Republic of Korea approved the studies.

Whole-Exome Sequencing and Whole-Genome Sequencing

To identify genomic variants that cause SPONASTRIME, we performed WES. Additionally, whole-genome sequencing (WGS) was conducted in cases where only a single pathogenic *TONSL* allele was identified by WES (individuals P01-1 and P01-2). The basic statistics of the WES data are summarized in Table S2. On the basis of the inheritance pattern of the affected individuals, we hypothesized that the disease is inherited in an autosomal-recessive fashion. Thus, we eliminated variants that did not satisfy the following criteria: (1) the variants showed an allele frequency <1% in the National Heart, Lung, and Blood Institute (NHLBI) Exome Sequencing Project (ESP6500) and the 1000 Genomes Project; (2) the variants were not found in our in-house database; (3) the variants were protein-altering variants; and (4) the variants had a high quality of reads (read number > 20, quality score (QS) > 30, or minor-allele frequency (MAF) > 20%). The resulting list of variants is displayed in Table S3. For the structural variants from WGS data, we used Manta (0.20.2) with the default settings and Control-FREEC (6.4) for identifying copy-number variants (CNVs) (see Web Resources). In Control-FREEC, the window size was set as 10,000, and read counts were normalized on the basis of GC-content bias. CNV type was classified on the basis of a genome ploidy value of 2; values below 2 denoted loss, and values above 2 denoted gain.

Amino Acid Conservation and Base-Level Functionality Analyses

To evaluate the functionality of nine missense variants in *TONSL*, we downloaded orthologous sequences from 61 mammalian species from the UCSC Browser and aligned them with human TONSL. The CADD and GERP scores across *TONSL* coding sequences were downloaded from dbNSFP.[17]

Long-Range PCR

We conducted long-range PCR (LR-PCR) to analyze the *TONSL* exon 23 deletion found in individuals P01-1, P01-2, and their mother by using the following primers: TONSL-exon22-F: 5′-GAA GAGACTGCCAAGCCAAG-3′ and TONSL-exon24-R: 5′-TACCATT TCTGTGGCCCTTC-3′.

Sanger Sequencing

The sequencing of *TONSL* candidate variants that were found with WES or WGS analysis was conducted via standard PCR and Sanger sequencing methods (primer sequences available upon request). The sequence data were aligned to the reference sequence in Sequencher software (Gene Codes).

Reverse Transcription-PCR and Cloning

To investigate both the splicing changes caused by the splicing site and deep intronic mutations in individual P11, we performed reverse transcription-PCR (RT-PCR) and cloned the amplicon. The proband's and parents' mRNA was harvested from circulating leukocytes with the QIAamp RNA Blood Mini Kit (QIAGEN). cDNA was transcribed with the Transcriptor First Strand cDNA Synthesis Kit, and then PCR amplification was carried out with the primers TONSL4F 5′-TATGACCACTGCCAGTCGAG-3′ and TONSL11R 5′-TGAGCTCCCGTAGTCTGGTT-3′, which encompass both paternal and maternal mutations. After PCR-based cloning was performed with an All in One PCR Cloning Kit (Biofact), we picked 30 colonies for PCR and sequencing analyses conducted with the same primers.

Cell Culture, Cell Immortalization, Mutagenesis, and TONSL Cell Line Establishment

Dermal fibroblasts from affected individuals were grown in high-glucose and no-glutamine DMEM (GIBCO, 10313) supplemented with 15% fetal bovine serum (FBS; GIBCO), glutamine (GIBCO, 35050-061), minimum essential medium (MEM) non-essential amino acid (GIBCO, 11140-050), and penicillin and streptomycin (GIBCO, 15140-122), and they were grown in 5% CO_2 and 3% O_2 at 37°C. We used BJ foreskin fibroblasts obtained from ATCC as a normal control. HeLa, U2OS, and 293T cells were grown in high-glucose DMEM (GIBCO, 11965) supplemented with 10% FBS and penicillin and streptomycin (GIBCO, 15140-122), and they were grown in 5% CO_2 at 37°C. Dermal fibroblasts from affected

individuals were transformed by the human papilloma virus E6 and E7 (HPV16 E6E7) protein and immortalized by the catalytic subunit of human telomerase (hTERT) through retroviral transduction. HPV16 E6E7 genes (a gift from Howley Lab, Harvard Medical School) were subcloned into pMSCVneo (Clontech) and used for transforming the dermal fibroblasts. pWZL-hTERT was used to immortalize the dermal fibroblasts from the affected individuals. The gene-coding wild-type (WT) TONSL was amplified from a cDNA library prepared from U2OS cells by PCR with the following primers: TONSL-F (5′-GGGGACAAGTTTGTACAAAAA AGCAGGCTTAATGAGCCTGGAGCGCGAGC-3′) and TONSL-R (5′-GGGGACCACTTTGTACAAGAAAGCTGGGTCTCAGAGGCGC CGAAAGAAGAGC-3′). The PCR product was cloned into a Gateway BP vector, pDONR223, with BP clonase. The pDONR223 clone was sequenced and then recombined into pHAGE vectors with LR clonase (Thermo Fisher Scientific). Using the pDONR223-TONSL template, we generated the point mutation plasmids used in this study with the QuikChange II XL Site-Directed Mutagenesis Kit (Agilent Genomics). The primers we used to generate *TONSL* mutations are listed in Table S5.

Fiber Analysis

For replication-fork stalling, cells from individual P03 were pulse-labeled with 25 μM 5-chloro-20-deoxyuridine (CldU: Sigma-Aldrich C6891), washed with PBS, pulse-labeled with 250 μM 5-iodo-20-deoxyuridine (IdU; Sigma-Aldrich I7125), and harvested. The cells were washed and resuspended to 5×10^5 cells/mL in PBS. The cells were lysed in spreading buffer (200 mM Tris-HCl [pH 7.5], 50 mM EDTA, 0.5% SDS) on glass slides. The DNA fibers were spread by gravity, then fixed with methanol:acetic acid (3:1) denatured with 2.5M HCl. CldU was detected with rat anti-BrdU antibody (clone BU1/75, ICR1; Abcam, ab6326; 1:750) and IdU with mouse anti-BrdU antibody (clone B44; BD Biosciences, 347583; 1:750). Slides were fixed with 4% paraformaldehyde, then stained with Alexa Fluor 594- or 488-conjugated secondary antibodies (Life Technologies). Images were acquired with a Nikon Eclipse Ni microscope with 60× oil-immersion objectives and NIS-Elements software (Nikon Instruments). Replication fork structures (>1000 fork structures) and CldU/IdU track lengths (>300 ongoing forks) were analyzed in ImageJ software (US National Institutes of Health [NIH]). For CPT treatment (DNA damage repair) fiber analysis, cells were treated with 100 μM CldU for 30 min, then 250 μM 5-iodo-20-deoxyuridine (IdU; Sigma-Aldrich I7125) for 30 min with 2.5 μM/50 nM CPT or DMSO. We prepared a DNA plug with by $\sim 2 \times 10^5$ to 4.5×10^5 cells/plug by using low-melting agarose (Bio-Rad 161-3112), followed by lysis with 20 mg/mL Proteinase K (Roche 03115828001) for two days at 50°C. For the stretching of DNA fibers, 22 mm × 22 mm silanized coverslips (Genomic Vision) were dipped into the DNA solution for 13 min and pulled out at a constant speed (300 μM/s) with a Molecular Combing System (Genomic Vision MCS-001). The coverslips were baked for 4 h at 60°C and incubated with acid for denaturation. For detection of CldU- and IdU-labeled, the coverslips were incubated for 2 h at room temperature (RT) with rat anti-BrdU antibody (dilution 1:100 detects BrdU and CldU; Abcam 6326) and mouse anti-BrdU antibody (1:10, detects BrdU and IdU; Becton Dickinson 347580). The slides were fixed in 4% paraformaldehyde in PBS and incubated for 1 h at RT with Alexa Fluor 488-conjugated goat anti-rat antibody (dilution 1:100, A21208; Molecular Probes/Thermo Fisher) or Alexa Fluor 568-conjugated goat anti-mouse antibody (dilution 1:100, A21124; Molecular Probes/Thermo Fisher). Finally, they were mounted with ProLong Gold Antifade Reagent (Molecular Probes) and stored at −20°C. DNA fibers were observed with Carl Zeiss Axio Observer 7 and ApoTome 2 (motorized fluorescence microscope with grid projection) 63 objective lenses. For each experiment, a total of 200 DNA fibers were analyzed; the number of DNA fibers was measured with ImageJ.

siRNA Transfection, Cell Proliferation, and CPT Sensitivity Assay

The siRNA targeting *TONSL* coding regions are listed in Table S6. Here, 3×10^5 cells were plated in six-well plates and transfected with siRNA in reverse transfection manner. The cells were transfected a second time after 24 h. Then, 48 h after the second transfection, 4,000 cells were plated in four wells (12-well plates, SPL) for cell counting, and 1,000 cells were plated in four wells (96-well plates, Corning #3603) for Hoechst staining. The cells in the 12-well plates were counted with a Z1 Coulter Particle Counter (Beckman Coulter), and the nuclei of the Hoechst-stained cells in the 96-well plates were counted with Cytation 3 (BioTek). Then, 1,000 cells were plated in four wells in 96-well plates and were treated 24 h after plating with increasing concentrations of CPT. The cells were counted 5 days after treatment. The cells were then stained with Hoechst and counted with Gen 5 (BioTek). For cell lines from affected individuals, 40,000 cells/well were plated in six-well plates. After 24 h, cells were treated in triplicate with increasing concentrations of CPT (0–32 nM). 4 days after drug treatment, the cells were passed 1:4 to six-well plates; then they were counted 4 days later with a Z1 Coulter Particle Counter (Beckman Coulter).[18]

Immunoblot

We prepared cell lysate by boiling cells for 5 min in 2× SDS sample buffer (RBC) at 95°C. We used 7.5% precast gels (Bio-Rad) for the resolution of the proteins. Immunoblotting was performed with anti-HA (Biolegend; MMS-101R, Lot B224726), anti-TONSL (Bethyl: A303-843A, Lot #1), anti-GAPDH (Santa Cruz: SC-25778, Lot K0615), anti-phosphorylated checkpoint kinase 1 (CHK1) (Cell Signaling: 2348P, Lot #11), anti-phosphorylated checkpoint kinase 2 (CHK2) (Cell Signaling: 2661P, Lot #11), and anti-α-Tubulin (Abfrontier: LF-PA0146, Lot MJL01-02) antibodies to detect each protein.

Immunofluorescence (BrdU/Rad51)

For immunofluorescence, 3×10^5 cells were plated in six-well plates (SPL) with cover glass. For HeLa and U2OS cells, siRNA was treated in a reverse and forward transfection manner and plated 48 h after the second transfection. For BrdU incorporation, 24 h after plating, the cells were treated with BrdU (20 μg/mL) for 4 h, then fixed with 3.7% formaldehyde in PBS. The Invitrogen protocol was followed. Cells were washed in PBS and fixed in 3.7% formaldehyde in PBS for 15 min. After being washed in PBS, the cells were permeabilized in 0.1% Triton X-100 buffer for 20 min, then in 1N HCl for 10 min on ice. The cells were then incubated in 2N HCl for 10 min at RT, then in phosphate citric acid buffer for 10 min. Cells were washed in permeabilization buffer twice, then incubated with Alexa-Fluor-488-conjugated anti-BrdU primary antibody overnight at RT. For Rad51 and γ-H2A.X immunofluorescence, 24 h after plating, the cells were treated with CPT (500 μM) overnight, then fixed in 3.7% formaldehyde for

15 min, then permeabilized with 0.1% Triton X-100 for 20 min with PBS washing in between. After being washed with PBS twice, the cells were blocked with PBG (0.2% [w/v] cold fish gelatin, 0.5% BSA in PBS) for 1 h at RT. Then, the cells were incubated in PBG overnight at 4°C with 1:7000 of anti-Rad51 antibody (Abcam, ab133534, Lot #: GR219215-36) and 1:1000 anti-γ-H2A.X antibody (Cell Signaling, #9718S, Lot #13). The following day, the cells were washed three times with PBG and incubated with fluorescent-conjugated secondary antibody for 30 min. Secondary antibodies were purchased from Abcam (Ms Alexa Fluor 594: ab150112; Rb Alexa Fluor 594: ab150064; Ms Alexa Fluor 488: ab150109; and Rb Alexa Fluor 488: ab150061). After being washed with PBG three times, the coverslips were embedded in Vectashield (Vector Laboratories) supplemented with DAPI. Imaging was performed with a Nikon A1 confocal microscope equipped with a CFI-Apochromat 60× NA-1.4 oil objective lens, the A1-DUG GaAsP multi detector unit, and the NIS-Element C-ER software. For the BrdU assay, the ratio was calculated by dividing the number of BrdU-incorporated cells by the number of total cells counted.

Animals and Ethics Statement

All mice were purchased from Taconic Biosciences (Dae Han Biolink) and housed at the specific pathogen-free (SPF) facility of the Yonsei Laboratory Animal Research Center. Animal experimental procedures were conducted in accordance with the Korean Food and Drug Administration (KFDA) guidelines, reviewed, and approved by the institutional animal care and use committees (IACUC) at Yonsei University (Permit Number: 201506-322-02).

Preparation of CRISPR-Cas9 mRNA and Donor DNA

Cas9 mRNA was synthesized with a mMESSAGE mMACHINE T7 Ultra kit (Ambion) and diluted to working concentration in endonuclease-free injection buffer (0.25 mM EDTA, 10 mM Tris [pH 7.4]) immediately before microinjection. A plasmid encoding the *S. pyogenes* Cas9 (SpCas9) protein[19] was obtained from ToolGen. The crRNAs were designed by searching for "NGG" or "CCN" (the reverse complement sequence of NGG) sequences near the point mutation target sites. The crRNA sequences used in this study were as follows: crRNA1 5′-GGTCCAGCCCCCTCCCATCC-3′, crRNA2 5′-GAACCCGGATGGGAGGGGGC-3′, crRNA3 5′-CCGGGTTCGAGTTCAAATTC-3′, and crRNA4 5′-CCTGAATTTGAACTCGAACC-3′. The 106 bp synthesized single-stranded oligonucleotide (ssDNA) we used as donor DNA was c.T2770C (p.Arg924Trp) ssDNA 5′-TAGAAACTTCTGTCTTCTGACTGTCCCCTCCCTCTGTCTTTCCTGCTAGCTTCTGGTCCAGCCTCCTCCTATCTGGGTTCGGGTTCAGATTCAGGATAACCTTTTCCTCATCCCCGTTCCC-3′. The tracrRNA, the crRNAs targeting the *Tonsl* gene, and the ssDNA donor for homology-directed repair were obtained from Integrated DNA Technologies (IDT).

Microinjection

Microinjection of one-cell embryos was performed as previously described.[20] In brief, 3–4-week-old C57BL/6 female mice were superovulated by intra-peritoneal (i.p.) injections of 5 IU pregnant mare serum gonadotropin (PMSG, Sigma) and 5 IU human chorionic gonadotropin (hCG, Sigma) at 48 h intervals. The superovulated females were then crossed with stud males, and the fertilized eggs were collected and microinjected with a mixture of Cas9 mRNA (50 or 100 ng/μL), four crRNAs (10, 25, or 50 ng/μL each), tracrRNA (tracrRNA mixed with crRNA at 1:1 molar ratio), and donor ssDNA (200 ng/μL). The microinjections were performed in the cytoplasm of one-cell embryos with a piezo-driven manipulator (Prime Tech) and followed by embryo transfer into the oviducts of pseudo-pregnant ICR mice to produce a living mouse.

Founder Screening and Genotyping PCR

To screen founders carrying the p.Arg924Trp mutation in the *Tonsl* gene, we performed a PAGE-PCR) assay as previously described[21] with genomic DNA obtained from newborns that were produced from the microinjected embryos. In brief, the genomic regions spanning the crRNA target site were amplified by PCR. After simply denaturing and annealing the PCR products, we analyzed the resulting products via acrylamide gel electrophoresis. Then, the candidates were cloned in T-Blunt PCR Cloning Vector (SolGent) and were validated by direct sequencing analysis (Cosmobiotech). The primer sequences we used in PAGE-PCR were as follows: forward, 5′-TGAATGCAGAGCCTGCAGAGA-3′ and reverse, 5′-TCTAGGGAGCAGAGTGCCAAG-3′. For genotyping PCR, DNA was extracted from tails or yolk sacs. We used the forward primer 5′-AAGCAGTCTTCAGCATGGGACT-3′ and the reverse WT primer 5′-AACTCGAACCCGGATG-3′ to identify the *Tonsl* WT allele. We used forward primer 5′-AAGCAGTCTTCAGCATGGGACT-3′ and reverse KI primer 5′-ACCCAGATAGGAGGAG-3′ to identify the *Tonsl* p.Arg924Trp allele. The reverse WT primer is annealed specifically to the sequence of the *Tonsl* WT allele, whereas the reverse KI primer is annealed to the sequence of the Tonsl p.Arg924Trp allele.

Embryo Collection

Gestation was dated by the detection of a vaginal plug (as E0.5), or after *in-vitro* fertilization (IVF) and embryo transfer. The embryos were either fixed in 10% neutral buffered formalin (Sigma-Aldrich) or snap-frozen in liquid nitrogen. Stereomicroscope images were generated from specimens of fixed embryos.

Results

Diagnosis and the Clinical Information of Individuals with SPONASTRIME Dysplasia

We recruited 13 individuals, including one whose case had previously been reported,[10] satisfying the diagnostic criteria of the disease from four different ethnicities—Korean, Indian, Finnish, and Brazilian (African black and non-Latin European). Their clinical features are presented in Table 1 and in the Supplemental Case Reports. The median height standard deviation score (SDS) for the individuals in this study was −4.9; the SDS ranged from −0.9 to −10.0, showing a wide range from mild to severe short stature. All the recruited individuals shared similar facial dysmorphism (Figure 1A). Other clinical findings shared by more than one individual included a short dental root, airway narrowing, cataracts, and joint laxity. Radiographic features were characterized by distinct changes in the vertebrae and the metaphyses of the long bones. It is worth noting that the radiographic features changed and became more conspicuous with age (Figure 1B and Table S1).

Table 1. Clinical Features of Individuals in This Series

ID	P01-1[a]	P01-2[a]	P02	P03	P04	P05	P06	P07[b]	P08	P09	P10	P11	P12
Ethnicity	Korean	Korean	Korean	Korean	Brazilian (African black and non-Latin European)	Korean	Finnish	Korean	Indian	Indian	Indian	Korean	Indian
Age of Initial Presentation	8 years, 5 months	6 years	2 months	13 years	2 years, 2 months	2 years, 7 months	newborn	36 years	13 years	14 years	11 years	3 years, 5 months	1 year, 9 months
Gender	f	m	m	m	m	f	f	m	m	f	f	f	f
Consanguinity	no	no	no	no	yes	no	no	no	no	no	no	no	no
Initial Presentation	short stature	short stature	short stature	radiographic abnormality of the knee	short stature	short stature	short stature	neck and shoulder pain	short stature	short stature	short stature and limb deformity	short stature	short stature
Height at First Measurement (cm) (SDS)	104.1 (−3.6)	93.4 (−4.7)	47.9 (−4.9)	145.2 (−0.9)	76 (−4.0)	74 (−4.5)	40 (−5.6)	136 (−6.2)	120 (−4)	119 (−7)	93 (−10)	73.6 (−5.6)	53 (−10)
Age at Latest Measurement	17 years, 5 months	15 years	5 years, 7 months	N/A	13 years	6 years	12 years, 6 months	37 years	13 years	14 years	11 years	4 years, 2 months	2 years
Latest Height (cm) (SDS)	124.4 (−6.8)	143.5 (−4.8)	82.6 (−6.0)		122 (−4.6)	98.8 (−3.4)	85.8 (−10.4)	136 (−6.2)	120 (−4)	119 (−7)	93 (−10)	80.6 (−5.8)	
Facial Dysmorphism	(+)	(+)	(+)	(+)	(+)	(+)	(+)	(+)	(+)	(+)	(+)	(+)	(+)
Cognitive Impairment	(−)	(−)	(−)	(−)	borderline	(−)	(−)	(−)	(−)	(−)	(−)	(−)	(−)
Other Findings	short dental roots	short dental roots	hypothyroidism; nystagmus; hypospadias; airway narrowing[c]		recurrent pneumonia in the 1st year; short dental roots	hypothyroidism; recurrent pneumonia until age 5 years; precocious puberty	cataracts; cerebro-vascular aneurysm rupture; weak voice	Arnold-Chiari malformation; cataracts	N/A	N/A	joint laxity	joint laxity; hip subluxation; airway narrowing[c]	

Abbreviations are as follows: m = male, f = female, SDS = standard deviation score, and N/A = not available.
[a]These two individuals are siblings.
[b]Previously reported (Jeong et al.[10]).
[c]Airway narrowing was composed of glottic narrowing and diffuse tracheal narrowing.

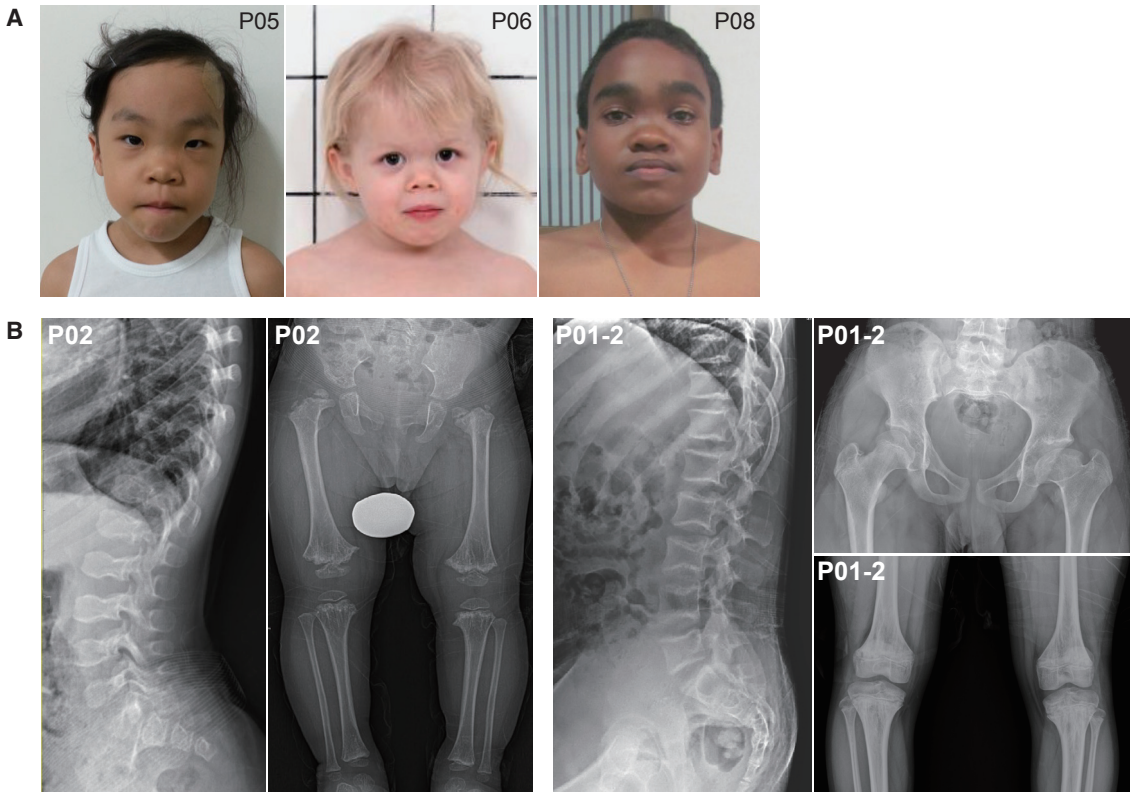

Figure 1. Characteristic Facial Appearance and Radiographic Findings of Individuals with SPONASTSRIME Dysplasia
(A) Facial photos of individuals from three different ethnicities. They share midfacial hypoplasia, a depressed nasal root, a short and upturned nose, prognathism, and a relatively large head size with a prominent forehead. Individual P05 is shown at age 5 years, individual P06 at age 5 years, and individual P08 at age 13 years.
(B) A lateral spine view of individual P02 at age 3 years and 8 months shows a taller anterior vertebral body and convex anterior endplates. A lateral spine view of individual P01-2 at age 13 years shows biconcavity of the endplates. Hip and knee anteroposterior views of individual P02 show metaphyseal irregularity and vertical striation and small, dysplastic epiphyses. Hip and knee anteroposterior views of individual P01-2 show residual avascular necrosis of the left femoral head and mixed dense striations and lucent area at the metaphysis of the knee.

Identification of TONSL Mutations in Individuals with SPONASTRIME Dysplasia

To identify the pathogenic mutation causing the disease, we conducted WES of eight affected individuals and available family members from seven families (five Koreans, one Brazilian, and one Finnish; individuals P01-1 to P07) (Tables S2 and S3). On the basis of the hypothesis that this disease is inherited in an autosomal-recessive manner, we retrieved rare variants (<1% frequency in the public databases) that were specifically harbored by the probands among the eight individuals with homozygous or compound-heterozygous status. Among the individual-specific variants that followed a recessive pattern, variants in *TONSL* were present in four individuals (Table 2). The remaining four individuals harbored single variants in the gene and required further analysis so that we could verify whether they also fit into the recessive model. For example, subsequent WGS analysis of the sibling probands (individuals P01-1 and P01-2) identified an exon 23 deletion in the maternal allele; this deletion was validated by PCR. Next, an additional cohort from India was recruited and subjected to singleton WES (individuals P08 to P10), which led to the discovery of bi-allelic variants in *TONSL*. Finally, we screened two additional individuals (one Korean and one Indian) for such *TONSL* variants by Sanger sequencing and identified bi-allelic mutations in one (individual P11) and a single mutation in the other (individual P12). Individual P11 has a splicing site variant and a deep intronic variant whose subsequent changes in mRNA were confirmed by RT-PCR. Only one mutation was identified in the *TONSL* gene in the three probands P05, P06, and P12 (Table 2). Because the parents who were harboring the same mutation were unaffected, it is highly likely that the affected individuals had undetermined variants, such as a cryptic structural variation or a noncoding variation, in the remaining *TONSL* allele. All the *TONSL* mutations identified were confirmed by Sanger sequencing (Figures S1A and S1B). No significant variation was found in other skeletal-dysplasia-related genes in affected individuals. Ten out of thirteen affected individuals (76.9%) carried one LoF allele and one missense allele (Table 2). Except for nonsense mutations, which might lead to nonsense-mediated mRNA decay, *TONSL* missense mutations were found in various locations throughout the protein-coding region (Figure 2A), mostly within functionally annotated

Table 2. *TONSL* Mutations and Their Predicted Protein Changes Identified in 13 Individuals

ID	Mutation 1		Mutation 2		Genetic Study
P01-1[a]	exon 23 deletion[b]		c.2800C>T	p.Arg934Trp	quad WES
P01-2[a]	exon 23 deletion[b]		c.2800C>T	p.Arg934Trp	quad WES
P02	c.1531C>T	p.Gln511*	c.2917G>A	p.Gly973Arg	trio WES
P03	c.735C>G / c.737delT[c]	p.Cys245Trpfs*20	c.1615G>A	p.Glu539Lys	trio WES
P04	c.1673G>A	p.Arg558Gln	c.1673G>A	p.Arg558Gln	trio WES
P05	c.1090G>C	p.Asp364His	not identified	not identified	quad WES
P06	c.578+1G>T	N/A	not identified	not identified	trio WES
P07[g]	c.2907C>A	p.Tyr969*	c.3862G>C	p.Glu1288Gln	singleton WES
P08	c.1471_1472delTC	p.Ser491Argfs*65	c.521G>A	p.Ser174Asn	singleton WES
P09	c.1459G>A / c.1989_1991del[d]	p.Glu487Lys / p.664delLeu	c.125G>A	p.Arg42His	singleton WES
P10	c.295delT	p.Ser99fs*59	c.1459G>A	p.Glu487Lys	singleton WES
P11	c.578+1G>A	p.Thr151Argfs*42[e]	c.1291–11_1291–14delCCTC	p.Arg431Profs*6 / p.431_441del[f]	Sanger sequencing
P12	c.1459G>A	p.Glu487Lys	not identified	not identified	Sanger sequencing

Abbreviations are as follows: WES = whole-exome sequencing.
[a]These two individuals are siblings.
[b]g.145657122_145658684del.
[c]Paternal allele harbors a substitution followed by a deletion of one nucleotide.
[d]Paternal allele harbors a substitution and an in-frame deletion.
[e]RT-PCR revealed an mRNA sequence change, predicting a truncated protein or nonsense-mediated mRNA decay.
[f]RT-PCR and cloning its products revealed WT (14/25) and two different mutant mRNAs formed by retention of a part of intron 10 (5/25) and by skipping of a part of exon 11 (6/25); these alterations predicted these two different polypeptides.
[g]P07 had two mutations that were confirmed to be bi-allelic by testing his siblings because his parents had already passed away. All other individuals with two or three mutations were confirmed to be bi-allelic by testing their parents.

domains (8 out of 9). The nine missense variants displayed complete or near-complete evolutionary conservation across vertebrate species (Figure 2B) and were found in low frequency in the healthy population (5/9 were not found in the ExAC database; all nine $< 1.0 \times 10^{-4}$). To predict the functionality of the missense variants, the CADD and GERP scores were compared with the rest of the amino acid residues of the protein, and they displayed significant differences (Figures 2C and S2A–2D). *TONSL* is tolerant to LoF variants (ExAC pLI = 0.00), but no individual in this study carried LoF variants in both alleles, implying a critical but minimal requirement of TONSL function for survival.

Complementation of Defects in Dermal Fibroblasts from Individuals by Expression of Wild-Type TONSL

In an attempt to validate that TONSL variants are causal for the SPONASTRIME phenotype, we established primary dermal fibroblast lines from two individuals, P03 and P04. Immunoblot analysis showed a pronounced decrease in TONSL levels compared to those in normal human fibroblasts (BJ cells) (Figure 3A). siRNA treatment abrogated endogenous TONSL protein levels (Figures 3A and S5A). To further validate the causative nature of TONSL variants, we transduced an empty vector (EV) and HA-tagged WT TONSL into P03 and P04 cells (Figure 3B) and performed functional complementation assays. Expressing WT-*TONSL* successfully rescued the cells' enhanced sensitivity to CPT (Figure 3C) and the DNA-damage-induced RAD51-foci formation in both cell lines (Figures 3D and 3E). As controls for the CPT sensitivity assay, we used BJ cells and FANCP cells (also known as SLX4), which are *SLX4*-deficient dermal fibroblasts that were, in this case, derived from an individual with Fanconi anemia. The FANCP cells were found to be sensitive to CPT; this sensitivity was rescued by introducing WT SLX4 protein through lentiviral transduction.[18,22] The CPT sensitivity assays of P03 and P04 cells were designed similarly to that of the previous FANCP cell assay, but they included EV and WT TONSL-complemented cells. In addition to the normal control BJ cells, we used EV and WT SLX4 FANCP cells for comparing CPT sensitivity. Also, to confirm the impaired DNA replication caused by the TONSL variants found in affected individuals, a BrdU-incorporation assay was performed and quantified by immunofluorescence. As expected, the BrdU incorporation ratios in P03/EV and P04/EV cells were less than that in BJ cells, whereas the complemented cells showed increased BrdU incorporation (Figure 3F). In a study by Duro et al., it was reported that although *TONSL* knockdown cells are sensitive to CPT, they are not sensitive to hydroxyurea (HU) compared to control cells.[6] In order to test whether the fibroblasts from individuals with mutant *TONSL* display similar characteristics, we treated P03 and P04 cells with HU. Consistent with previous reports, neither P03 nor P04 cells were sensitive to HU

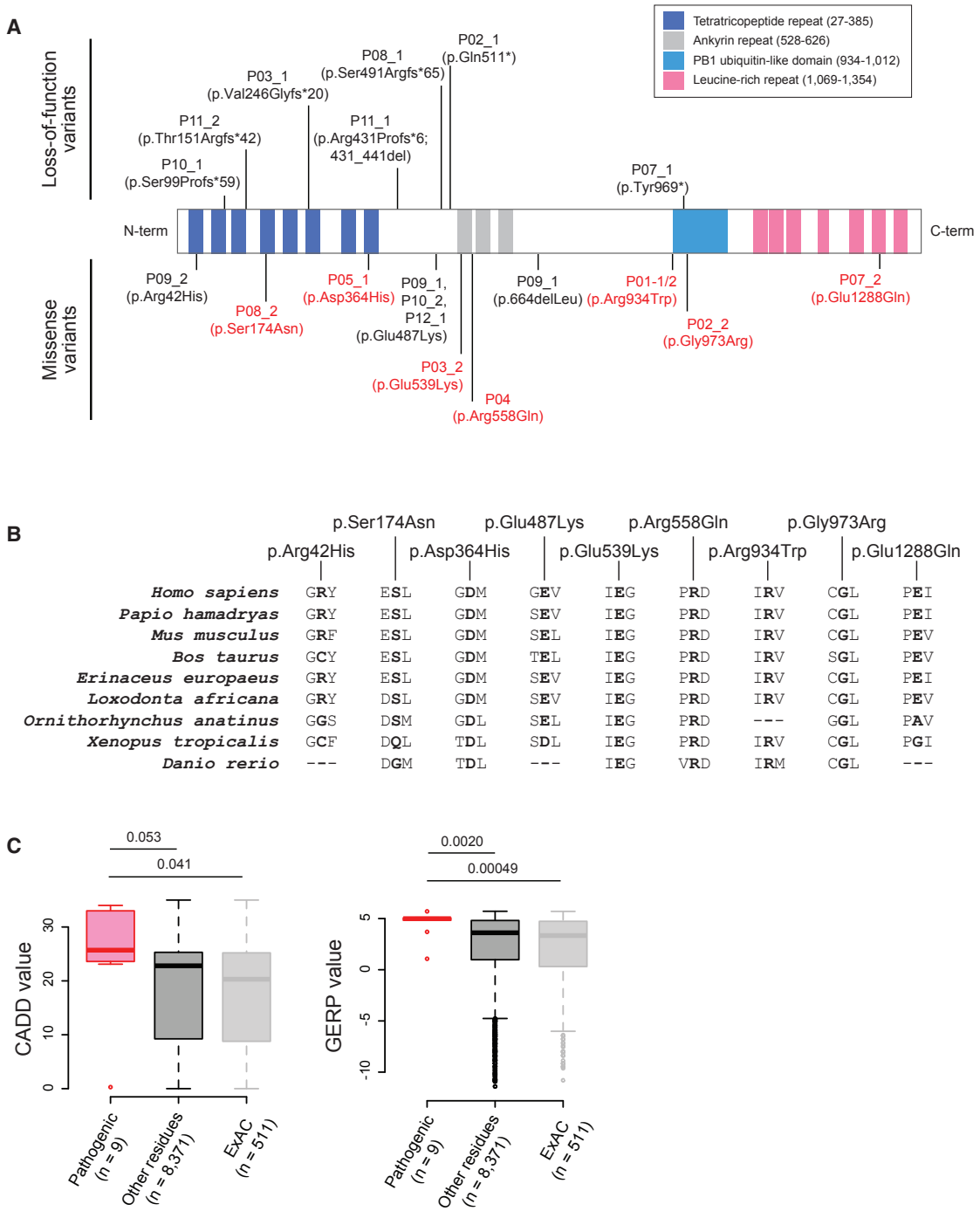

Figure 2. TONSL Variants Identified in Individuals with SPONASTRIME Dysplasia
(A) Pathogenic variants in TONSL found in SPONASTRIME-affected individuals are displayed on the TONSL protein, whose known functional domains are indicated. Variants in red were analyzed for variant functionality.
(B) Evolutionary conservation of the nine missense variants found in SPONASTRIME-affected individuals.
(C) Because they are parameters of an individual's missense-variant ("Pathogenic") functionality, CADD and GERP values were plotted, along with residues that overlapped with the ExAC Database ("ExAC") and residues that were not polymorphic ("Other residues").

(Figure S3). As mentioned earlier, TONSL is involved in homologous recombination, and its impairment results in decreased cell proliferation and increased sensitivity to CPT.[12,13] Because homologous recombination is an important part of DNA damage repair, and thus DNA replication, it is possible that TONSL variants might increase the occurrence of stalled replication forks as a result of defects in DNA damage repair. In order to evaluate the mutant *TONSL's* impairment of replication restart and DNA damage repair, we performed fiber analysis with fibroblasts from individual P03 and with normal control cells (Figure S4). We used the nucleotide analogs CldU

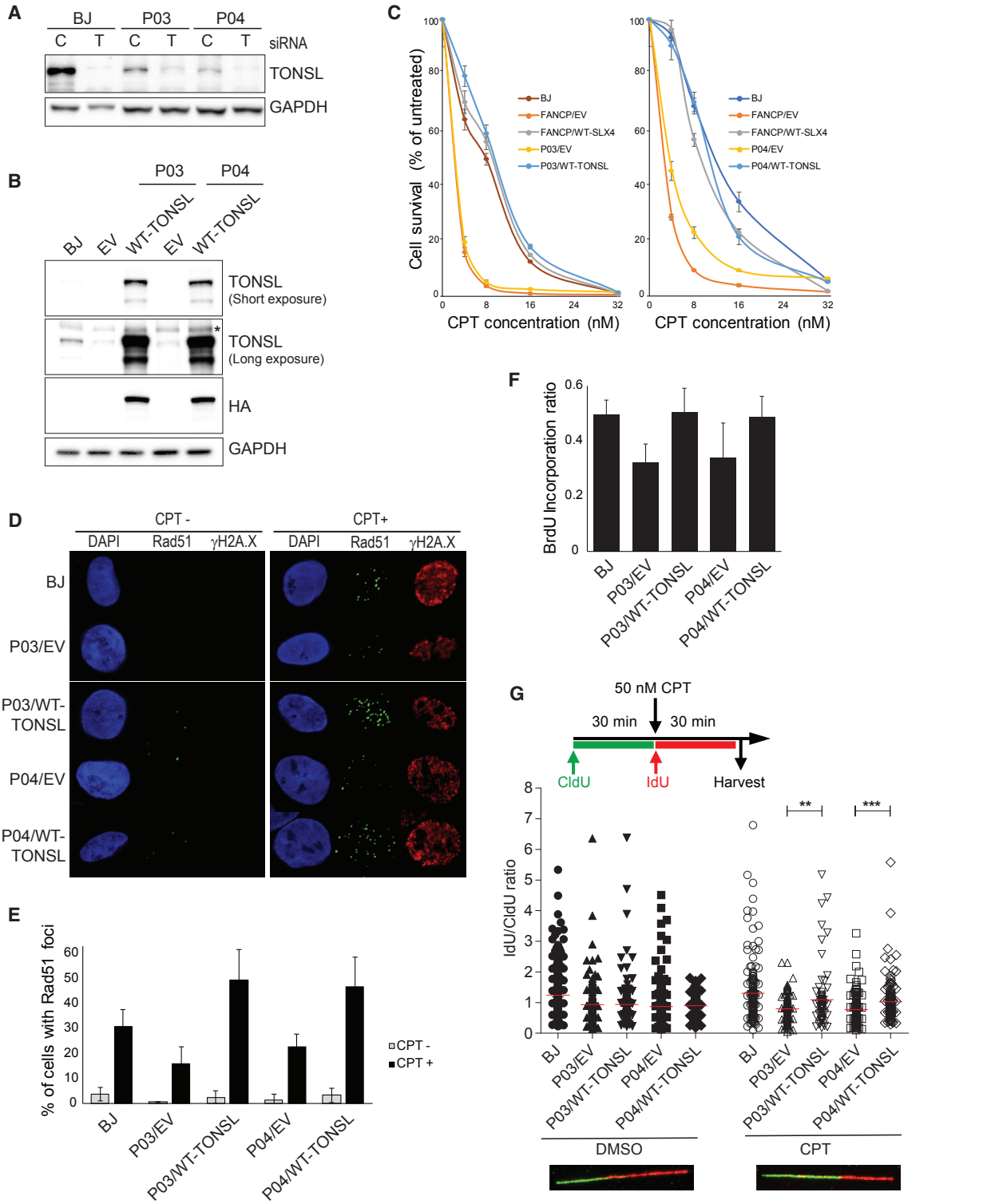

Figure 3. Complementation of Dermal Fibroblasts from Individuals P03 and P04 through *TONSL* cDNA Transduction

(A) TONSL protein levels and corresponding siRNA-mediated *TONSL* depletion of cells from individuals with SPONASTRIME dysplasia. BJ cells were used as a normal control. The basal TONSL level in cells derived from the affected individuals was lower than that in BJ cells, and all of the cells were successfully depleted by siRNA treatment. C = siControl and T = siTONSL.

(B) Stable protein level of wild-type (WT) TONSL delivered through lentiviral transduction into fibroblasts derived from both individuals P03 and P04. EV and WT denote the empty vector and wild-type, respectively. The asterisk indicates the cross-reacting band.

(C) Cells from affected individuals were sensitive to CPT but were rescued to a level comparable to that of BJ cells by the transduction of WT TONSL. The indicated cells, in triplicate, were exposed to different concentrations of CPT ranging from 0–32 nM. After 5 days, the cells were counted with a coulter counter, and the total number of cells at each concentration was divided by the number of untreated

(legend continued on next page)

and IdU to track the newly synthesized DNA from the first label origin and the second label origin, respectively. Ongoing forks have both CldU and IdU tracks, whereas stalled forks can be monitored by CldU-only labeled tracks. To compare the changes in ongoing or stalled replication forks, we calculated the percentage of CldU and IdU tracks from the total of all CldU-incorporated tracks. Compared to in a normal human fibroblast, the percentage of ongoing replication forks was slightly decreased in P03 cells, and the number of stalled forks was significantly (Figure S4). Next, we performed fiber analysis for CPT sensitivity in P03 and P04 cells and we used EV, WT-TONSL, and BJ cells as controls. When treated with 50 nM of CPT, P03/EV and P04/EV cells showed decreases in replication length compared to that in BJ cells; these decreases were rescued by WT-TONSL (Figure 3G). Taken together, these data provide strong evidence that the TONSL variants found in affected individuals impair DNA replication and repair capacity; these impairments were all rescued by WT-TONSL, thus demonstrating the pathogenic nature of *TONSL* mutations in the disease phenotype.

Validation of Pathogenic TONSL Mutations in *In Vitro* Cell-Based Assay

To systematically evaluate the pathogenicity of *TONSL* variants found in other individuals whose primary fibroblasts were not available, we established an *in vitro* cell-based assay using HeLa cell lines. We focused on missense *TONSL* mutations because nonsense mutations might be subject to nonsense-mediated mRNA decay. First, we tested whether we could recapitulate the results of previous reports showing that TONSL depletion leads to enhanced sensitivity to CPT.[11,12] In order to accomplish this, we established an assay system in which mutant *TONSL* is expressed in a HeLa cell line, but the endogenous WT is selectively knocked down. The strategy was to establish via lentiviral transduction individual HeLa cell lines that stably express each mutant *TONSL* variant, then treat the cells with siRNA targeting the *TONSL* 3′ untranslated region (UTR); this process selectively knocks down only the endogenous *TONSL* mRNA. If successful, the HA-tagged *TONSL* is expressed, and any cellular defects arising from *TONSL* mutation can be observed without the interference of the endogenous *TONSL*. WT-TONSL and EV cell lines were established as positive and negative controls, respectively. To first test the siRNAs, we treated HeLa cells with siRNA targeting the coding region and the 3′ UTR. As shown in Figures S5A and S5B, depleting TONSL by targeting the coding or the 3′ UTR region in HeLa cells resulted in hypersensitivity to CPT. Then, HeLa cells that stably expressed the individual EV, HA-tagged WT-*TONSL,* and the HA-tagged *TONSL* missense mutation were successfully established (Figure S5C). The siRNA targeting the *TONSL* 3′ UTR selectively knocked down endogenous *TONSL*, but not HA-tagged WT or mutant *TONSL* (Figure 4A). After confirming the selective knockdown of endogenous *TONSL* and decreased TONSL protein levels, we treated EV, WT-TONSL, and TONSL variant cells with siRNA targeting the *TONSL* 3′ UTR, then grew the cells for 5 days to monitor cell proliferation. Overall, a noticeable proliferation defect was observed in TONSL-variant HeLa cells compared to WT-TONSL cells (Figure 4B). Of these, proliferation of cells with the P02 c.2917G>A, (p.Gly973Arg), P01-1 and P01-2 c.2800C>T (p.Arg934Trp), P05 c.1090G>C (p.Asp364His), and P08 c.521G>A (p.Ser174Asn) variants were significantly inhibited to a similar level as that of siTONSL-treated HeLa-EV cells (Figure 4B). This result shows that all examined TONSL variants directly impact cell proliferation, but to varying degrees. At the same time, we evaluated phosphorylated CHK1 and CHK2 after endogenous TONSL depletion in the individual TONSL-variant HeLa cells. We found that the checkpoint is activated in cells with proliferation defects (Figure 4C), suggesting that the functional impairment of TONSL leads to genome instability, which results in cell-cycle arrest and inhibition of cell division. To further investigate the role of each TONSL variant in repairing replication-associated DNA damage, we performed a CPT sensitivity assay. Consistent with the proliferation results, the CPT sensitivity of the TONSL variant cells was comparable to that of siTONSL-treated HeLa-EV cells, which lack TONSL (Figure 4D). In addition, we modeled the WT and TONSL variants on the basis of the existing available structure to determine the basis of

cells. FANCP/EV, a Fanconi anemia-derived cell line lacking *Slx4*, and FANCP/WT-SLX4, a genetically isogenic line of SLX4-complemented cells, were used as controls. The error bars represent the standard deviation (SD) of three replicates.
(D) Representative images of CPT-induced DNA damage in Rad51 and γH2A.X foci. P03/EV, P03/WT-TONSL, P04/EV, and P04/WT-TONSL cells were treated with CPT (50 nM) overnight, then fixed and stained with anti-RAD51 and anti-γH2A.X antibodies. Impaired DNA damage induced RAD51 foci formation in those cells from affected individuals that were recovered to the level of normal cells via the transduction of WT-TONSL.
(E) Statistical analysis of Rad51 foci. The percentage of Rad51 foci was calculated by taking the number of nuclei with $n \geq 10$ Rad51 foci divided by the total number of nuclei from non-treated cells, or, for CPT-treated cells, divided by the number of γH2A.X-positive nuclei. The error bars represent the SD.
(F) BrdU incorporation into DNA was reduced in P03/EV and P04/EV cells, which were rescued to a normal level by the transduction of WT-TONSL. The BrdU incorporation ratio was calculated by dividing the number of BrdU-incorporated cells by the number of total cells counted. The error bars represent the SD of three replicates.
(G) DNA fiber analysis of CPT-treated cell lines derived from SPONASTRIME-affected individuals. BJ cells were used as a control. A schematic representation of the experiment is shown on the top, and the representative DNA fiber is shown on bottom. The red line indicates median value; ** $p = 0.003$ and *** $p < 0.001$.

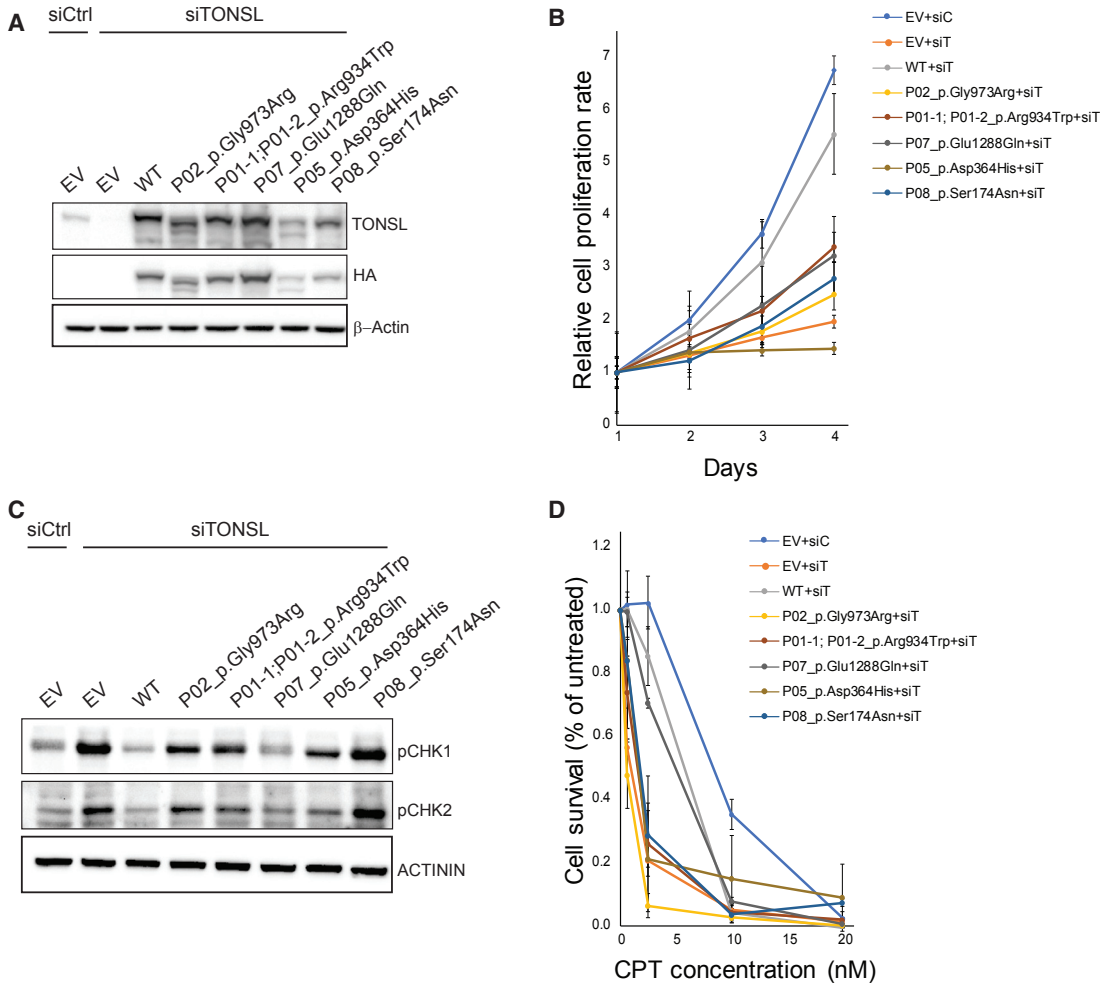

Figure 4. ***In Vitro*** **Cell-Based Assay of TONSL Variants Shows Defects in Cell Proliferation and Enhanced Sensitivity to Camptothecin**
(A) The protein levels of recombinant WT and TONSL variants from affected individuals transduced and stably expressed in HeLa cells upon endogenous TONSL depletion via siRNA that targeted the *TONSL* 3′ UTR. The TONSL antibody is able to detect both endogenous and HA-tagged TONSL, whereas the HA antibody is not able to detect endogenous TONSL. The asterisk indicates the cross-reacting band.
(B) Cell-proliferation assay showing the varied proliferation rates of cells expressing mutant *TONSL*. EV cells were treated with either non-targeting siCtrl or siTONSL targeting the 3′ UTR. The rest of the cells were treated with siTONSL targeting the 3′ UTR. The cell proliferation rate was normalized to the cell number on day 1. The error bar represents the SD of three replicates. siCtrl = siControl.
(C) TONSL variants in the absence of endogenous TONSL lead to checkpoint activation. Whole-cell extracts of HeLa cells expressing mutant *TONSL* were treated with siRNA targeting the 3′ UTR and analyzed by immunoblot with DNA-damage-response factors, phosphorylated CHK1 (pCHK1), or phosphorylated CHK2 (pCHK2).
(D) TONSL variant cell lines were treated with 3′ UTR-targeting siRNA as in (B), then treated with increasing concentrations of CPT. The cells were stained with Hoechst, and the nuclei were counted 5 days after CPT treatment. Cell survival was normalized to that in vehicle-treated cells. The error bars represent the SD from three replicates.

the aberrant function of the TONSL variants (Figure S6). c.1615G>A (p.Glu539Lys) (P03) and c.1673G>A (p.Arg558Gln) (P04) altered the polar interactions between amino acids. Exon 23 deletion from individuals P01-1 and P01-2 changed the curvature of the LRR domain significantly, and c.1989_1991del (p.664delLeu) (P09) altered the direction of the C terminus of the helix (Figures S6A–G). These changes deformed the overall structures, and such changes might influence binding affinity between variant TONSL and its binding partners (Figure S6). From the studies implementing *in vitro* cell-based assay and *in silico* structural analyses, we conclude that the identified TONSL variants compromise TONSL functional activity, and that this compromise potentially leads to human diseases.

Embryonic Lethality of the Tonsl Knock-In Mouse Model

To better understand the pathophysiology and clinical correlations, we generated a CRISPR-Cas9-mediated Tonsl KI mouse carrying a p.Arg924Trp substitution (akin to its human counterpart TONSL p.Arg934Trp variant found in individuals P01-1 and P01-2) in *Tonsl* (Figures 5A–C and S7A). Heterozygous *Tonsl*$^{+/Arg924Trp}$ (HT) mice were fertile and showed normal gross morphology. Intriguingly, no offspring littermates (n = 38) carrying the bi-allelic p.Arg924Trp variant were obtained from heterozygous

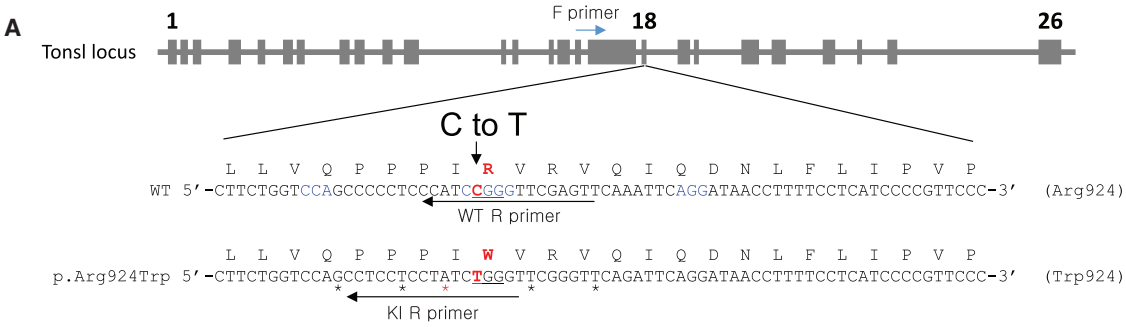

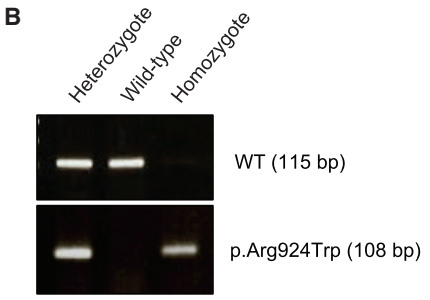

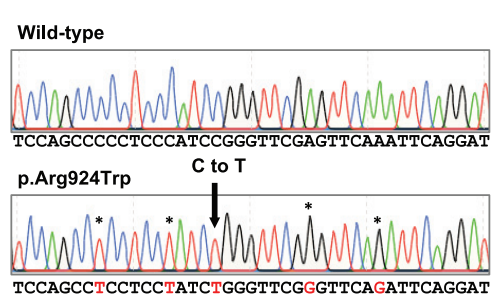

D

Line	Litters	No. of mice	Wild-type + / +	Heterozygotes + /p.Arg924Trp	Homozygotes p.Arg924Trp/p.Arg924Trp	Female	Male
A	4	27	6	21	0	15	12
B	2	11	4	7	0	6	5
A+B	6	38	10	28	0	21	17
Ratio			1	2.8	0	1	0.8

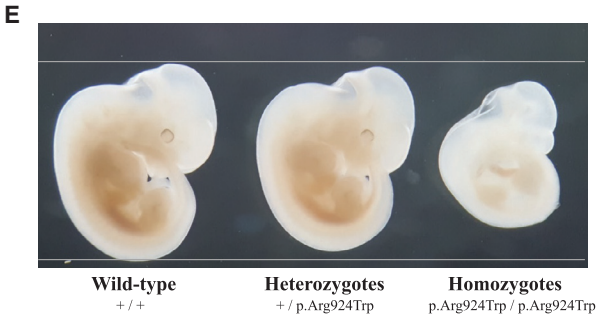

Figure 5. Generation and Analysis of Homozygous Tonsl p.Arg924Trp Knock-In Mice via CRISPR-Cas9
(A) A schematic diagram showing the mouse *Tonsl* locus and the enlarged sequences of exon 18 of t*Tonsl*, along with the sequences of the Tonsl^{Arg924Trp} allele. Blue letters in the Tonsl^{WT} allele indicate a proto-spacer adjacent motif (PAM) sequence. Red letters indicate the substitution (C to T) target nucleotide in the Tonsl^{WT} and the Tonsl^{Arg924Trp} alleles. The amino acid sequences from the Tonsl^{WT} and the Tonsl^{Arg924Trp} alleles are shown at the top of the nucleotide sequences. The substituted nucleotides for both synonymous and targeted mutations are shown at the bottom of the Tonsl^{Arg924Trp} allele sequences by black and red asterisks (*), respectively. Forward (F) and Reverse (R) PCR primers for genotyping are indicated.
(B) Genotyping PCR for the Tonsl^{WT} and the Tonsl^{Arg924Trp} alleles. The upper and bottom panels show the PCR products that were amplified from the Tonsl^{WT} (115 bp) and the Tonsl^{Arg924Trp} (108 bp) alleles, respectively.
(C) Chromatogram displaying the sequence of the Tonsl^{WT} and the Tonsl^{Arg924Trp} loci.
(D) Genotype distribution of offspring from heterozygous intercrosses.
(E) Gross morphology of whole embryos at stage E11.5. *Tonsl*$^{+/+}$ and *Tonsl*$^{+/Arg924Trp}$ mouse embryos show normal development, whereas a *Tonsl*$^{Arg924Trp/Arg924Trp}$ embryo exhibits a growth retardation with the abnormal development of eyes and limbs.

intercrosses, although their WT and HT littermates were born in a 1:2.8 ratio (Figure 5D), suggesting that the homozygotes were not viable. For development analysis, we collected embryos from embryonic days 10.5 to 12.5 (E10.5–E12.5) and observed a 1:1.4:0.6 ratio of WT:HT:KI embryos (Table S4). However, all homozygous *Tonsl*$^{Arg924Trp/Arg924Trp}$ embryos showed early embryonic lethality along with fetal growth restriction at around E10.5 (Figures 5E and S7B–D). The yolk sacs of homozygous *Tonsl*$^{Arg924Trp/Arg924Trp}$ embryos lacked visible blood

vessels and were smaller than others (Figure S7E). Consistent with *in vitro* cell-based assays of the human TONSL p.Arg934Trp variant, these results suggest that the Tonsl p.Arg924Trp variant is not functional, and that the lack of this functional protein is likely the major reason for embryonic lethality. Taken together, these findings demonstrated the physiological importance of functional Tonsl protein in embryonic development and the pathogenic nature of the TONSL p.Arg934Trp variant.

Discussion

In this study, we report the identification of *TONSL* mutations causative for SPONASTRIME dysplasia in 13 individuals. We demonstrate that the endogenous TONSL protein level in dermal fibroblast cells from the presented individuals with SPONASTRIME dysplasia is significantly lower than that in WT control cells. Furthermore, we found that the cells from affected individuals exhibit enhanced sensitivity to CPT, reduced DNA-damage-induced RAD51-foci formation, and impaired replication capacity, all of which are successfully rescued by WT-TONSL through lentiviral transduction. Given the importance of TONSL function in replication-fork stability during normal S phase,[23] it is reasonable to speculate that pathogenic *TONSL* variants result in impaired cell proliferation, which is critical for embryonic development and postnatal growth.[24] Similarly, mutations in various genes important for preventing replication-associated DNA lesions have been identified in individuals with growth retardation.[22,24,25]

In cells with a TONSL variant, we found increased phosphorylation of CHK1 and CHK2 (Figure 4C) in the absence of endogenous TONSL or siRNA-mediated TONSL depletion, even without treatment with genotoxic agents. CHK1 is mainly phosphorylated by ATR (Ataxia-telangiectasia and Rad3-related protein), and deleterious mutations in the *ATR* (MIM:601216) gene result in Seckel syndrome (MIM: 210600), which is characterized by microcephaly, dwarfism, progeria, and intellectual disability.[25,26] ATR responds to a many types of DNA damage, and together with ATR-interacting protein (ATRIP), recognizes RPA bound to ssDNA, which is often the result of a stalled replication fork.[27] We observed that mutations in *TONSL* did not affect the formation of RPA foci in response to CPT-induced DNA damage in cells from individuals with SPONASTRIME dysplasia (unpublished data), implying that TONSL functions downstream of ATR activation. Therefore, it is possible to speculate that alterations in ATR, which functions upstream of TONSL, might lead to broader defects, whereas loss of TONSL function might cause milder disease phenotypes such as SPONASTRIME dysplasia. It remains unknown why alterations in *TONSL* result specifically in SPONASTRIME dysplasia and understanding the genotype-to-phenotype correlation requires further study.

Our KI mouse model clearly demonstrated that even a single point mutation, p.Arg924Trp (corresponding to p.Arg934Trp identified in human SPONASTRIME dysplasia), causes embryonic lethality in mice. Although this finding in the mouse model does not directly translate to the pathogenicity of human disease, it provides evidence supporting the hypothesis that the TONSL p.Arg934Trp variant might be causative of SPONASTRIME dysplasia, and it highlights the physiological importance of TONSL. The homozygous p.Arg924Trp variant in mouse Tonsl has severe developmental impact: fetal growth retardation was observed at approximately E10.5 and resulted in embryonic lethality. However, the heterozygotes surviving to adulthood showed no apparent defects. Consistent with the *in vitro* cell-based assay (Figures 4B–D), these results suggest that Tonsl proteins carrying the p.Arg924Trp variant are not functional and that the lack of this functional protein is considered to be the main reason for embryonic lethality in the Tonsl KO mouse (B. Lee, personal communication) and even our KI models. However, unlike in mice, the human TONSL p.Arg934Trp variant is found in a subgroup of individuals with SPONASTRIME dysplasia. The discrepancy between human and mouse phenotypes might be due to the difference in transcript isoforms found in humans and mice. According to the GENCODE basic project,[28] two transcripts are predicted to be translated in humans, whereas mice only have one transcript. Among the two transcripts in humans, the shorter isoform lacks the domain containing the Arg934 residue, as well as the UBL and LRR domains. Whether the shorter isoform has any function in humans has yet to be elucidated, but the possibility that it provides partial function for survival cannot be excluded. More research is needed to understand the TONSL variants because the presence of another TONSL isoform could have prevented lethality in humans. Although further study is required if we are to understand how the decreased function of TONSL leads to the specific phenotype of SPONASTRIME dysplasia, we believe that our findings increase our understanding of the pathogenesis of this disease.

Accession Numbers

The raw genome data can be downloaded at http://biodata.kr/ (Submission ID: 1711075636).

Supplemental Data

Supplemental Data include Supplemental Case Reports, Supplemental Material and Methods, Supplemental References, seven figures, and six tables and can be found with this article online at https://doi.org/10.1016/j.ajhg.2019.01.009.

Acknowledgments

We are grateful to the affected individuals, their families, and the clinicians for their invaluable contribution. We thank the Smogorzewska Lab, Rockefeller University, New York, New York, USA for reagents; Dr. Je Hoon Jeong for providing the genomic DNA for individual P07; and Thatiane Y. Kanazawa for

contributing to the fibroblast culture of individual P04. This research was supported by the Genome Technology to Business Translation Program of the National Research Foundation (NRF) funded by the Ministry of Science, ICT & Future Planning (NRF-2014M3C9A2064684 to T.J.C. and NRF-2014M3C9A2064688 to Y.K.); by an NRF grant funded by the Korean government (NRF-2017R1A2B4003147 to Y.K.; NRF-2016R1A5A1011974 to Y.K. and M.S.L.; 2017R1A4A1015328 to H.W.L.; and 2015R1A2A1A01003845 to H.W.L.); by Samsung Medical Center (#GFO2170061 to S.Y.C.); partly by the Department of Science and Technology, India, for the project "Application of autozygosity mapping and exome sequencing to identify genetic basis of disorders of skeletal development" (SB/SO/HS/005/2014 to K.M.G.); by the Academy of Finland (No.318137 to O.M.); by KAKENHI (Grants-in-Aid for Scientific Research) (No.17K16710 to Z.W.); by the Japan Agency For Medical Research and Development (AMED: No.JP17ek0109280 to S.I.); by the National Key Research and Development Program of China; by RIKEN-MOST China (2016YFE0128400 to S.I. and Z.W.); by the São Paulo Research Foundation (FAPESP) (#2015/22145-6 to D.P.C.); and by the Centre for Molecular Medicine at the Sanjay Gandhi Post Graduate Institute of Medical Sciences (SGPGIMS) (Grant number 63/8/2010-BMS to S.R.P.). Dr. Outi Mäkitie has an affiliation with Folkhälsan Institute of Genetics, Helsinki, Finland.

Declaration of Interests

The authors declare no competing interests.

Received: August 10, 2018
Accepted: January 17, 2019
Published: February 14, 2019

Web Resources

Control-FREEC, http://boevalab.com/FREEC/
ExAC Browser, http://exac.broadinstitute.org/
Online Mendelian Inheritance in Man, http://www.omim.org
Protein Data Bank, https://www.rcsb.org/
UCSC Browser, http://genome.ucsc.edu

References

1. Fanconi, S., Issler, C., Giedion, A., and Prader, A. (1983). The SPONASTRIME dysplasia: Familial short-limb dwarfism with saddle nose, spinal alterations and metaphyseal striation. Report of 4 siblings. Helv. Paediatr. Acta *38*, 267–280.
2. Lachman, R.S., Stoss, H., and Spranger, J. (1989). Sponastrime dysplasia. A radiologic-pathologic correlation. Pediatr. Radiol. *19*, 417–424.
3. Langer, L.O., Jr., Beals, R.K., LaFranchi, S., Scott, C.I., Jr., and Sockalosky, J.J. (1996). Sponastrime dysplasia: Five new cases and review of nine previously published cases. Am. J. Med. Genet. *63*, 20–27.
4. Masuno, M., Nishimura, G., Adachi, M., Hotsubo, T., Tachibana, K., Makita, Y., Imaizumi, K., and Kuroki, Y. (1996). SPONASTRIME dysplasia: Report on a female patient with severe skeletal changes. Am. J. Med. Genet. *66*, 429–432.
5. Langer, L.O., Jr., Beals, R.K., and Scott, C.I., Jr. (1997). Sponastrime dysplasia: Diagnostic criteria based on five new and six previously published cases. Pediatr. Radiol. *27*, 409–414.
6. Nishimura, G., Mikawa, M., and Fukushima, Y. (1998). Another observation of Langer-type sponastrime dysplasia variant. Am. J. Med. Genet. *80*, 288–290.
7. Cooper, H.A., Crowe, J., and Butler, M.G. (2000). SPONASTRIME dysplasia: Report of an 11-year-old boy and review of the literature. Am. J. Med. Genet. *92*, 33–39.
8. Offiah, A.C., Lees, M., Winter, R.M., and Hall, C.M. (2001). Sponastrime dysplasia: Presentation in infancy. J. Med. Genet. *38*, 889–893.
9. Umpaichitra, V., Wallerstein, R., and Castells, S. (2002). Sponastrime dysplasia with abnormal urinary glycosaminoglycans and growth hormone unresponsiveness. Clin. Dysmorphol. *11*, 53–56.
10. Jeong, J.H., Lee, A.L., Cho, S.Y., Jin, D.K., and Im, S.B. (2016). Arnold Chiari malformation with sponastrime (spondylar and nasal changes, with striations of the metaphyses) dysplasia: A case report. Medicine (Baltimore) *95*, e3155.
11. O'Donnell, L., Panier, S., Wildenhain, J., Tkach, J.M., Al-Hakim, A., Landry, M.C., Escribano-Diaz, C., Szilard, R.K., Young, J.T., Munro, M., et al. (2010). The MMS22L-TONSL complex mediates recovery from replication stress and homologous recombination. Mol. Cell *40*, 619–631.
12. Duro, E., Lundin, C., Ask, K., Sanchez-Pulido, L., MacArtney, T.J., Toth, R., Ponting, C.P., Groth, A., Helleday, T., and Rouse, J. (2010). Identification of the MMS22L-TONSL complex that promotes homologous recombination. Mol. Cell *40*, 632–644.
13. O'Connell, B.C., Adamson, B., Lydeard, J.R., Sowa, M.E., Ciccia, A., Bredemeyer, A.L., Schlabach, M., Gygi, S.P., Elledge, S.J., and Harper, J.W. (2010). A genome-wide camptothecin sensitivity screen identifies a mammalian MMS22L-NFKBIL2 complex required for genomic stability. Mol. Cell *40*, 645–657.
14. Piwko, W., Olma, M.H., Held, M., Bianco, J.N., Pedrioli, P.G., Hofmann, K., Pasero, P., Gerlich, D.W., and Peter, M. (2010). RNAi-based screening identifies the Mms22L-Nfkbil2 complex as a novel regulator of DNA replication in human cells. EMBO J. *29*, 4210–4222.
15. Saredi, G., Huang, H., Hammond, C.M., Alabert, C., Bekker-Jensen, S., Forne, I., Reverón-Gómez, N., Foster, B.M., Mlejnkova, L., Bartke, T., et al. (2016). H4K20me0 marks post-replicative chromatin and recruits the TONSL–MMS22L DNA repair complex. Nature *534*, 714–718.
16. Piwko, W., Mlejnkova, L.J., Mutreja, K., Ranjha, L., Stafa, D., Smirnov, A., Brodersen, M.M., Zellweger, R., Sturzenegger, A., Janscak, P., et al. (2016). The MMS22L-TONSL heterodimer directly promotes RAD51-dependent recombination upon replication stress. EMBO J. *35*, 2584–2601.
17. Liu, X., Wu, C., Li, C., and Boerwinkle, E. (2016). dbNSFP v3.0: A one-stop database of functional predictions and annotations for human nonsynonymous and splice-site SNVs. Hum. Mutat. *37*, 235–241.
18. Kim, Y., Spitz, G.S., Veturi, U., Lach, F.P., Auerbach, A.D., and Smogorzewska, A. (2013). Regulation of multiple DNA repair pathways by the Fanconi anemia protein SLX4. Blood *121*, 54–63.
19. Cho, S.W., Kim, S., Kim, J.M., and Kim, J.S. (2013). Targeted genome engineering in human cells with the Cas9 RNA-guided endonuclease. Nat. Biotechnol. *31*, 230–232.
20. Sung, Y.H., Kim, J.M., Kim, H.T., Lee, J., Jeon, J., Jin, Y., Choi, J.H., Ban, Y.H., Ha, S.J., Kim, C.H., et al. (2014). Highly efficient gene knockout in mice and zebrafish with RNA-guided endonucleases. Genome Res. *24*, 125–131.

21. Lee, J.H., Park, J.H., Nam, T.W., Seo, S.M., Kim, J.Y., Lee, H.K., Han, J.H., Park, S.Y., Choi, Y.K., and Lee, H.W. (2018). Differences between immunodeficient mice generated by classical gene targeting and CRISPR/Cas9-mediated gene knockout. Transgenic Res. *27*, 241–251.
22. Kim, Y., Lach, F.P., Desetty, R., Hanenberg, H., Auerbach, A.D., and Smogorzewska, A. (2011). Mutations of the SLX4 gene in Fanconi anemia. Nat. Genet. *43*, 142–146.
23. Piwko, W., Buser, R., and Peter, M. (2011). Rescuing stalled replication forks: MMS22L-TONSL, a novel complex for DNA replication fork repair in human cells. Cell Cycle *10*, 1703–1705.
24. Reynolds, J.J., Bicknell, L.S., Carroll, P., Higgs, M.R., Shaheen, R., Murray, J.E., Papadopoulos, D.K., Leitch, A., Murina, O., Tarnauskaitė, Ž., et al. (2017). Mutations in DONSON disrupt replication fork stability and cause microcephalic dwarfism. Nat. Genet. *49*, 537–549.
25. O'Driscoll, M., Ruiz-Perez, V.L., Woods, C.G., Jeggo, P.A., and Goodship, J.A. (2003). A splicing mutation affecting expression of ataxia-telangiectasia and Rad3-related protein (ATR) results in Seckel syndrome. Nat. Genet. *33*, 497–501.
26. Murga, M., Bunting, S., Montaña, M.F., Soria, R., Mulero, F., Cañamero, M., Lee, Y., McKinnon, P.J., Nussenzweig, A., and Fernandez-Capetillo, O. (2009). A mouse model of ATR-Seckel shows embryonic replicative stress and accelerated aging. Nat. Genet. *41*, 891–898.
27. Maréchal, A., and Zou, L. (2013). DNA damage sensing by the ATM and ATR kinases. Cold Spring Harb. Perspect. Biol. *5*, a012716.
28. Harrow, J., Frankish, A., Gonzalez, J.M., Tapanari, E., Diekhans, M., Kokocinski, F., Aken, B.L., Barrell, D., Zadissa, A., Searle, S., et al. (2012). GENCODE: The reference human genome annotation for The ENCODE Project. Genome Res. *22*, 1760–1774.